Mitochondrial maturation in the trophectoderm and inner cell mass regions of bovine blastocysts

Yoshihiro Hayashi[a], Shun Saito[a], Hanako Bai[a], Masashi Takahashi[b], and Manabu Kawahara[a]*

[a]Laboratory of Animal Genetics and Reproduction, Research Faculty of Agriculture, Hokkaido University, Sapporo 060-8589, Japan

[b]Global Station for Food, Land and Water Resources, Global Institution for Collaborative Research and Education (GI-CoRE), Hokkaido 060-0815, Japan

*Correspondence:

Dr. Manabu Kawahara, PhD

Laboratory of Animal Genetics and Reproduction, Graduate School of Agriculture, Hokkaido University, Sapporo 060-8589, Japan

Tel. / Fax: +81 11 706 2541

E-mail address: k-hara@anim.agr.hokudai.ac.jp

Abstract

Cellular differentiation induces various morphological changes, including elongation, in mitochondria. Preimplantation embryos have round-shaped mitochondria, characteristic of undifferentiated cells. However, there is controversy regarding the precise mitochondrial morphology in blastocyst embryos, which are generated from two cell lineages: undifferentiated inner cell mass (ICM) and differentiated trophectoderm (TE). This study attempted to precisely determine mitochondrial morphology in these two blastocyst regions. Transmission electron microscopy analyses were conducted using more than 1,000 mitochondria from blastocyst embryos. No significant differences were observed in the configuration of mitochondrial cristae and frequencies of hooded mitochondria, which are specific to embryos of livestock animals, between the ICM and TE. To accurately compare mitochondrial roundness between the ICM and TE, oblateness was calculated based on both the major and minor axes. Average oblateness was significantly greater in the TE than in the ICM ($P < 0.01$). These results indicate tissue-specific mitochondrial maturation with complete elongation in the TE at the blastocyst stage. Since mitochondrial elongation is closely associated with cellular metabolism and differentiation, the present study provides new insights for better understanding of early embryonic development in cattle.

Keywords: bovine, blastocyst, mitochondria, trophectoderm, inner cell mass, ultrastructure

1. Introduction

Mitochondria in eukaryotic cells synthesize adenosine triphosphate (ATP). In preimplantation development, the contribution of mitochondria is considered to be highly essential. A reduction in the number of mitochondria hampers embryonic development and results in decreased fertilization and developmental rates in embryos cultured *in vitro* [1–3]. Undifferentiated early embryos possess immature mitochondria that are characterized by a round shape and undeveloped cristae [4,5]. Likewise, embryonic stem cells contain morphologically immature mitochondria that differ from the mitochondria in differentiated somatic cells [6–8]. This series of morphological changes in mitochondria is known as mitochondrial maturation [9,10], which appears to enhance the energy demand in differentiating cells. One of the most obvious morphological changes is the elongation of the whole organelle [4,5].

During the transitions from the 2-cell to the 8-cell stage in preimplantation development, spherical mitochondria gradually change shape to become elongated mitochondria in humans [5], and cattle [11] . This morphological transformation continues until the early blastocyst stage in humans [4] and cattle [11]. However, mitochondria that are included in a blastocyst do not uniformly progress to elongation. It is believed that the mitochondria in the trophectoderm (TE) cells of a blastocyst elongate prior to those in the inner cell mass (ICM) in mice [12,13]. TE cells, the first differentiated cell lineage in mammalian development, are derived from undifferentiated blastomeres at the blastocyst stage. The TE gives rise to the placental tissue, whereas the ICM generates the fetus during early development. Similarly, embryonic stem cells isolated from the ICM comprise round-shaped mitochondria that differ from those of the blastocyst TE [7,8]. The first occurrence of elongated mitochondria in TE cells appears to be consistent in mammalian development.

However, several reports have argued that there are no differences in mitochondrial morphology between the TE and ICM in blastocysts of mice [14] and cattle [15]. This contradiction

may stem from the analytical approach used to study mitochondrial morphology. Given the ultrafine structure of cellular organelles including mitochondria, observation is primarily limited to transmission electron microscopy (TEM) [16–18]. TEM is an effective experimental method for direct observation of the mitochondrial ultrastructure; however, the extremely limited field of observation may be responsible for the diverse interpretation of experimental results. Therefore, we quantitatively evaluated mitochondrial elongation by examination of in more than 1,000 mitochondria in bovine blastocysts using TEM.

2. Materials and methods

2.1. Ethics approval

All experimental protocols were approved by the Regulatory Committee for the Care and Use of Laboratory Animals, Hokkaido University (Approved number: 15-0085).

2. 2. Preparation of bovine embryos

Bovine oocyte retrieval, *in vitro* oocyte maturation, fertilization, and subsequent *in vitro* embryo culture were performed as previously described [19]. Briefly,cumulus-oocyte complexes (COCs) retrieved from slaughterhouse-derived 19 Holstein ovaries were matured by culturing them in TCM-199 medium (Thermo Fisher Scientific, Waltham, MA, USA) supplemented with 5% (v:v) fetal bovine serum at 38.5°C in a humidified atmosphere with 5% CO_2 in air for 20 to 22 h. *In vitro*-matured oocytes were transferred to Brackett and Oliphant (BO) medium [20] containing 2.5 mM theophylline (Wako Pure Chemical Industries, Osaka, Japan) and 7.5 μg/mL heparin sodium salt (Nacalai Tesque, Kyoto, Japan). Frozen-thawed semen derived from a single Holstein bull was centrifuged in BO medium at 600 X g for 7 min and the spermatozoa isolated from the pellet were added to the COCs at a final concentration of 5×10^6 cells/mL. After 12 h of incubation, the COCs

including the presumptive zygotes were denuded by pipetting and then cultured in mSOFai medium (at 38.5°C, in a humidified atmosphere with 5% CO_2 and 5% O_2 in air for 8 days) [21] After *in vitro* culture for 1.5 (Day 1.5) and 8.0(Day 8.0), 2-cell embryos and expanded blastocysts were subjected to TEM analysis. Also, *in vitro* development rates of bovine embryos were commonplace values and equivalent to those observed in previous studies (Supplemental Table 1) [22,23]. COCs before *in vitro* maturation were used for TEM analysis of cumulus cells.

2.3. TEM

Embryos and COCs were fixed using 2.5% glutaraldehyde (TAAB Laboratories, Reading, UK) in 0.1 M phosphate buffer (pH 7.2) at 4 °C for 2 h. After post fixation in 1% osmium tetroxide (Nisshin EM., Tokyo, Japan) at 4 °C, the specimens were dehydrated using an ethanol series. After the removal of ethanol with propylene oxide (Nisshin EM), specimens were embedded in epoxy resin 812 (TAAB Laboratories, Reading). Semi-thin sections (500 nm) were cut for light microscopy and stained with 0.3% toluidine blue for deciding the observed areas. Ultra-thin sections (80 nm) were prepared using an ultramicrotome (ULTRACUTN, Reichert-Nissei, Buffalo, NY, USA), stained with 2% uranyl acetate (MERCK, Darmstadt, Germany) and lead citrate [24], and examined using TEM (JEM-2100, JEOL Tokyo, Japan). Three embryos per embryo stage (2-cell embryo and blastocyst) were prepared for TEM analysis, and for each embryo, three ultrathin sections were prepared, resulting in nine sections for each embryonic sample type. The sections used were not consecutive. For the analysis of cumulus cells, we examined 1,058 mitochondria in 124 cumulus cells around oocytes. All mitochondria within each ultrathin section were analyzed. The major and minor axes of each mitochondrion were determined using the ImageJ software (National Institutes of Health, https://imagej.nih.gov/ij/index.html). In the present study, the longest line marked the major mitochondrial axis, whereas the longest line vertical to the major axis was defined as the minor axis

(Fig. 1A). To precisely determine both the major and minor axes, measurements were adjusted to the diverse mitochondrial shapes in the TEM images. In particular, for bent-shaped mitochondria, the sum of two lines drawn from the bending point was regarded the major axis (Fig. 1B). For mitochondria with a node, the longest line across the node was regarded as the major axis (Fig. 1C). For hooded mitochondria, which are specifically reported in livestock animal embryos [15,25–28], the longest line in the whole mitochondrion was measured as the major axis as shown in Fig. 1D. Hooded mitochondria were counted separately when total mitochondrial numbers in the ICM and TE were determined (Table 1). ICM and TE cell regions were distinguished based on cell positions within the ultrathin blastocyst sections although individual cell types within the ICM or TE regions were not discriminable (Supplemental Fig 1).

Ultrastructural analysis of blastocyst mitochondria was performed based on oblateness, which was determined using the following formula [29,30]: oblateness $= \frac{a-b}{a}$, where a is the major axis and b is the minor axis.

When mitochondria are closer to the circular shape, the oblateness value approaches 0. We calculated the oblateness for ultrastructure of 6,115, 1781, 1,405, and 1,058 mitochondria in 2-cell stage embryos, ICM, TE, and cumulus cells. The average mitochondrial oblateness was compared among the 2-cell stage embryos, ICM, TE and cumulus cells. In all quantitative analyses, we evaluated, the frequency of hooded mitochondria, frequencies of cristae. types and oblateness values after observation of all the mitochondria in each ultrathin section analyzed.

2.4. Statistical analysis

Mitochondrial oblateness data were analyzed using Tukey's honestly significant difference test. Frequencies of hooded mitochondria and cristae type in the ICM and TE were compared using a chi-square test. All the statistical analyses were performed using the statistical analysis software, R

(Comprehensive R Archive Network). A *P*-value < 0.01 was considered statistically significant.

3. Results

3.1. Mitochondrial maturity based on morphological roundness

In terms of cell differentiation, immature mitochondria show globular forms with poorly developed cristae, which are sub-compartments of the inner mitochondrial membrane [8,31–35]. In contrast, mature mitochondria are flattened and elongated, with well-developed cristae. We observed mitochondria in 2-cell stage embryos and cumulus cells using TEM (Fig. 2). Mitochondria in 2-cell stage embryos were globular, whereas those in cumulus cells were flattened.

3.2. Mitochondrial morphological differences between the ICM and TE regions

Next, we investigated mitochondrial morphology in expanded blastocysts as well as in 2-cell embryos and cumulus cells. TEM analysis revealed distinct differences in the morphology of mitochondria in the ICM and TE of a blastocyst (Fig. 3). Whereas ICM mitochondria exhibited a round shape, TE mitochondria were more elongated. Cristae, are formed by the inner membranes of mitochondria. Two typical forms of cristae that were commonly observed in both the ICM and TE were bleb and lamellar types (Fig. 4). Bleb type cristae are immature compared to lamellar type cristae [36,37]. We quantified and compared the frequencies of these cristae types between the ICM and TE, considering a lack of cristae as the immature type. We found no significant differences between the ICM and TE (Fig 4.). In 2-cell stage embryos, we did not observe bleb- and lamellar-type cristae, as in the ICM and TE. As hooded mitochondria are considered to be associated with mitochondrial maturation [38,39] , we counted hooded mitochondria in both the ICM and TE regions. We found no significant difference in the frequency of hooded mitochondria between the two regions (Table 1).

3.3. Comparison of mitochondrial oblateness in the ICM and TE regions

To precisely evaluate the differences in mitochondrial roundness between 2-cell stage embryos, ICM, TE, and cumulus cells, oblateness was assessed. Oblateness was determined by observing the TEM images of 6,115, 1,781, 1,405, and 1,058 mitochondria in 2-cell stage embryos, ICM, TE, and cumulus cells, respectively (Fig. 5). The average oblateness value in the TE region was significantly greater than that in the ICM region (Fig. 5, $P < 0.01$). Additionally, the average oblateness value was the lowest in 2-cell stage embryos and the highest in cumulus cells (Fig. 5, $P < 0.01$).. Furthermore, distribution of dot (i.e., distribution of oblateness value of a single mitochondrion) of TE resembled that of cumulus cells. These results demonstrated that the mitochondria in the TE region are more elongated than those in the ICM region, indicating that the former are in a more differentiated state.

4. Discussion

Morphological changes in the mitochondria of TE cells at the blastocyst stage during preimplantation development remain controversial [12–15]. We conducted a precise morphological evaluation of mitochondria in bovine blastocysts and revealed significant differences in mitochondrial ultrastructure between the ICM and TE regions in the blastocysts (Fig. 5). TE cells are derived from the pluripotent cell lineage and precede ICM cells in mitochondrial maturation Therefore, the elongated morphology of mature mitochondria observed in TE cells is consistent with the conventional concept that mitochondrial elongation is linked to cell differentiation, at least in mouse embryos [13,40].

The significance of mitochondrial elongation could stem from its implications in cellular metabolic development as it intrinsically extends the total area occupied by the surface of the mitochondrial membrane. The mitochondrial membrane serves as the site for ATP production by oxidative phosphorylation (OXPHOS); thus, its extension enhances cellular metabolism [41]. As mitochondria are multi-layered structures, mitochondrial elongation generally involves the development of cristae [42]. Although the average oblateness value was higher in the TE regions compared with that in the ICM region (Fig. 5), no obvious differences were noted in terms of mitochondrial cristae (Fig. 4). The development of cristae may be followed by mitochondrial elongation during preimplantation development in cattle.

Elongated mitochondria in TE cells may contribute to the metabolic alterations required for TE cell characterization. One of the basic functions of TE cells is blastocoel development through changes in ionic gradients, which are mainly accomplished by sodium-potassium adenosine triphosphatase (Na^+/ K^+-ATPase) [40,43]. Na^+/K^+-ATPase, which is localized on the basolateral membrane of TE cells, promotes Na^+ transport in the blastocoel in mice [44,45]. The movement of Na^+ is essential for adequate fluid accumulation and blastocyst expansion [46]. Blastocyst expansion

197 is considered to be the driving force for embryo hatching, which is essential for interactions between
198 the embryo and uterus during implantation. Moreover, Na^+/K^+-ATPase activation requires an
199 enormous amount of energy, which is 10% to 40% of the total energy consumed for blastocyst
200 expansion in cattle [47,48]. TE cells have been estimated to produce more than 80% of the ATP
201 generated in blastocysts [40]. Thus, the mitochondrial elongation observed in TE cells corroborates
202 with the increase in metabolism in this embryonic stage.
203 However, an understanding of how cell differentiation interacts with embryonic metabolism
204 remains obscure. Whereas pluripotent stem cells, including embryonic stem cells, produce ATP by
205 glycolytic metabolism, the metabolic pathway shifts from glycolysis to OXPHOS, depending on cell
206 differentiation [8,49]. Interestingly, this shift in ATP generation is concomitant with mitochondrial
207 elongation [41,50–52], Also, it has been suggested that different metabolic pathways operate
208 between the ICM and TE in bovine blastocysts [53,54]. Together with the findings in these
209 previous studies, the morphological assessments in the present study suggest an association between
210 mitochondrial elongation of TE cells and metabolic conversion. Although further research on
211 metabolism is required, our findings on mitochondrial morphology provide important clues for
212 understanding how cell differentiation interacts with embryonic metabolism.
213
214 **5. Conclusions**
215 We visualized morphological changes in mitochondria of bovine blastocysts using TEM.
216 Our morphological assessments revealed that mitochondria in the TE region are more elongated than
217 those in the ICM region; however, there was no difference in the shape of cristae between the two
218 regions. Although results from previous studies have generated, a controversy regarding
219 mitochondrial morphology in the ICM and TE regions, in the present study, we clearly demonstrate
220 that TE, rather than ICM, mitochondria resemble those of differentiated cells. In conclusion,

mitochondrial maturation during preimplantation development proceeds in a cell lineage specific manner.

Author Contributions

M.K. conceived the project. M.K. and Y.H. designed the experiments. Y.H. and S.S. conducted the experiments. H.B. and M.T. provided support in the preparation of the materials for the experiments. M.K. and Y.H. analyzed the data. M.K., H.B., and Y.H. drafted the manuscript. All authors contributed to the interpretation of the data and read and approved the final manuscript.

Declaration of Interest

The authors declare no conflicts of interest.

Acknowledgments

We would like to thank the Genetics Hokkaido Association for providing frozen bull spermatozoa and the Hokkaido Hayakita Meat Inspection Center and Nichiro Chikusan Co., Ltd. for providing bovine ovaries. We thank Toshiaki Ito, Electron Microscope Laboratory, Research Faculty of Agriculture, and Hokkaido University for helpful advice on TEM analysis. This work was funded by Grant-in-aid for Scientific Research (B) (18H02321 and 21H02336) to M.K.

References

[1] Spikings EC, Alderson J, St. John JC. Regulated mitochondrial DNA replication during oocyte maturation is essential for successful porcine embryonic development. Biol Reprod 2007;76:327–35. https://doi.org/10.1095/biolreprod.106.054536.

[2] Thouas GA, Trounson AO, Wolvetang EJ, Jones GM. Mitochondrial dysfunction in mouse oocytes results in preimplantation embryo arrest in vitro. Biol Reprod 2004;71:1936–42. https://doi.org/10.1095/biolreprod.104.033589.

[3] Chiaratti MR, Ferreira CR, Perecin F, Méo SC, Sangalli JR, Mesquita LG, et al. Ooplast-mediated developmental rescue of bovine oocytes exposed to ethidium bromide. Reprod Biomed Online 2011;22:172–83. https://doi.org/10.1016/j.rbmo.2010.10.011.

[4] Sathananthan AH, Trounson AO. Mitochondrial morphology during preimplantational human embryogenesis. Hum Reprod 2000;15:148–59. https://doi.org/10.1093/humrep/15.suppl_2.148.

[5] Motta PM, Nottola SA, Makabe S, Heyn R, Jansen R. Mitochondrial morphology in human fetal and adult female germ cells. Hum Reprod 2000;15:129–47. https://doi.org/10.1093/humrep/15.suppl_2.129.

[6] Cho YM, Kwon S, Pak YK, Seol HW, Choi YM, Park DJ, et al. Dynamic changes in mitochondrial biogenesis and antioxidant enzymes during the spontaneous differentiation of human embryonic stem cells. Biochem Biophys Res Commun 2006;348:1472–8. https://doi.org/10.1016/j.bbrc.2006.08.020.

[7] Folmes CDL, Nelson TJ, Martinez-Fernandez A, Arrell DK, Lindor JZ, Dzeja PP, et al. Somatic oxidative bioenergetics transitions into pluripotency-dependent glycolysis to facilitate nuclear reprogramming. Cell Metab 2011;14:264–71. https://doi.org/10.1016/j.cmet.2011.06.011.

[8] Varum S, Rodrigues AS, Moura MB, Momcilovic O, Easley IV CA, Ramalho-Santos J, et al. Energy metabolism in human pluripotent stem cells and their differentiated counterparts. PLoS

One 2011;6. https://doi.org/10.1371/journal.pone.0020914.

[9] Hom JR, Quintanilla RA, Hoffman DL, de Mesy Bentley KL, Molkentin JD, Sheu SS, et al. The permeability transition pore controls cardiac mitochondrial maturation and myocyte differentiation. Dev Cell 2011;21:469–78. https://doi.org/10.1016/j.devcel.2011.08.008.

[10] Dai DF, Danoviz ME, Wiczer B, Laflamme MA, Tian R. Mitochondrial maturation in human pluripotent stem cell derived cardiomyocytes. Stem Cells Int 2017;2017. https://doi.org/10.1155/2017/5153625.

[11] Plante L, King WA. Light and electron microscopic analysis of bovine embryos derived by in Vitro and in Vivo fertilization. J Assist Reprod Genet 1994;11:515–29. https://doi.org/10.1007/BF02216032.

[12] Mohr LR, Trounson AO. Comparative ultrastructure of hatched human, mouse and bovine blastocysts. J Reprod Fertil 1982;66:499–504. https://doi.org/10.1530/jrf.0.0660499.

[13] Kumar RP, Ray S, Home P, Saha B, Bhattacharya B, Wilkins HM, et al. Regulation of energy metabolism during early mammalian development: Tead4 controls mitochondrial transcription. Dev 2018;145:1–15. https://doi.org/10.1242/dev.162644.

[14] Choi J, Seo BJ, La H, Yoon SH, Hong YJ, Lee JH, et al. Comparative analysis of the mitochondrial morphology, energy metabolism, and gene expression signatures in three types of blastocyst-derived stem cells. Redox Biol 2020;30:101437. https://doi.org/10.1016/j.redox.2020.101437.

[15] Crosier AE, Farin PW, Dykstra MJ, Alexander JE, Farin CE. Ultrastructural morphometry of bovine blastocysts produced in vivo or in vitro 2001;1385:1375–85.

[16] Trebichalská Z, Kyjovská D, Kloudová S, Otevřel P, Hampl A, Holubcová Z. Cytoplasmic maturation in human oocytes: an ultrastructural study †. Biol Reprod 2021;104:106–16. https://doi.org/10.1093/biolre/ioaa174.

[17] Arismendi-Morillo G. Electron microscopy morphology of the mitochondrial network in gliomas and their vascular microenvironment. Biochim Biophys Acta - Bioenerg 2011;1807:602–8. https://doi.org/10.1016/j.bbabio.2010.11.001.

[18] Rybka V, Suzuki YJ, Gavrish AS, Dibrova VA, Gychka SG, Shults N V. Transmission electron microscopy study of mitochondria in aging brain synapses. Antioxidants 2019;8. https://doi.org/10.3390/antiox8060171.

[19] Nagatomo H, Kagawa S, Kishi Y, Takuma T, Sada A, Yamanaka K ichi, et al. Transcriptional Wiring for Establishing Cell Lineage Specification at the Blastocyst Stage in Cattle1. Biol Reprod 2013;88:1–10. https://doi.org/10.1095/biolreprod.113.108993.

[20] Reproduction C, Medicine V, September PA. of Rabbit. Biol Reprod 1975;274:260–74.

[21] Aono A, Nagatomo H, Takuma T, Nonaka R, Ono Y, Wada Y, et al. Dynamics of intracellular phospholipid membrane organization during oocyte maturation and successful vitrification of immature oocytes retrieved by ovum pick-up in cattle. Theriogenology 2013;79:1146-1152.e1. https://doi.org/10.1016/j.theriogenology.2013.02.009.

[22] Nagatomo H, Kohri N, Akizawa H, Hoshino Y, Yamauchi N, Kono T, et al. Requirement for nuclear autoantigenic sperm protein mRNA expression in bovine preimplantation development. Anim Sci J 2016;87:457–61. https://doi.org/10.1111/asj.12538.

[23] Akizawa H., Kobayashi K., Bai H., Takahashi M., Kagawa S. NH and KM. Reciprocal regulation of TEAD4 and CCN2 for the trophectoderm development of the bovine blastocyst. Reproduction 2018;155:563–71.

[24] Reynolds ES. The use of lead citrate at high pH as an electron-opaque stain in electron microscopy. J Cell Biol 1963;17:208–12. https://doi.org/10.1083/jcb.17.1.208.

[25] Crosier AE, Farin PW, Dykstra MJ, Alexander JE, Farin CE. Ultrastructural morphometry of bovine compact morulae produced in vivo or in vitro 2000;1465:1459–65.

[26] Dalcin L, Silva RC, Paulini F, Silva BDM, Neves JP, Lucci CM. Cytoskeleton structure, pattern of mitochondrial activity and ultrastructure of frozen or vitrified sheep embryos. Cryobiology 2013;67:137–45. https://doi.org/10.1016/j.cryobiol.2013.05.012.

[27] Paulini F, Silva RC, De Paula Rôlo JLJ, Lucci CM. Ultrastructural changes in oocytes during folliculogenesis in domestic mammals. J Ovarian Res 2014;7:1–12. https://doi.org/10.1186/s13048-014-0102-6.

[28] Reader KL, Stanton JAL, Juengel JL. The role of oocyte organelles in determining developmental competence. Biology (Basel) 2017;6:1–22. https://doi.org/10.3390/biology6030035.

[29] Barnes JW, Fortney JJ. Measuring the oblateness and rotation of transiting extrasolar giant planets. Astrophys J 2003;588:545–56. https://doi.org/10.1086/373893.

[30] Carter JA, Winn JN. The detectability of transit depth variations due to exoplanetary oblateness and spin precession. Astrophys J 2010;716:850–6. https://doi.org/10.1088/0004-637X/716/1/850.

[31] Prigione A, Fauler B, Lurz R, Lehrach H, Adjaye J. The senescence-related mitochondrial/oxidative stress pathway is repressed in human induced pluripotent stem cells. Stem Cells 2010;28:721–33. https://doi.org/10.1002/stem.404.

[32] Mandal S, Lindgren AG, Srivastava AS, Clark AT, Banerjee U. Mitochondrial function controls proliferation and early differentiation potential of embryonic stem cells. Stem Cells 2011;29:486–95. https://doi.org/10.1002/stem.590.

[33] Prowse ABJ, Chong F, Elliott DA, Elefanty AG, Stanley EG, Gray PP, et al. Analysis of Mitochondrial function and localisation during human embryonic stem cell differentiation in vitro. PLoS One 2012;7. https://doi.org/10.1371/journal.pone.0052214.

[34] Baharvand H, Matthaei KI. The ultrastructure of mouse embryonic stem cells. Reprod Biomed Online 2003;7:330–5. https://doi.org/10.1016/S1472-6483(10)61873-1.

[35] Sathananthan H, Pera M, Trounson A. The fine structure of human embryonic stem cells. Reprod

Biomed Online 2002;4:56–61. https://doi.org/10.1016/S1472-6483(10)61916-5.

[36] Shepard TH, Muffley LA, Smith LT. Ultrastructural study of mitochondria and their cristae in embryonic rats and primate (N. nemistrina). Anat Rec 1998;252:383–92. https://doi.org/10.1002/(SICI)1097-0185(199811)252:3<383::AID-AR6>3.0.CO;2-Z.

[37] Prince FP. Lamellar and tubular associations of the mitochondrial cristae: Unique forms of the cristae present in steroid-producing cells. Mitochondrion 2002;1:381–9. https://doi.org/10.1016/S1567-7249(01)00038-1.

[38] Mohr LR, Trounson AO. Structural changes associated with freezing of bovine embryos. Biol Reprod 1981;25:1009–25. https://doi.org/10.1095/biolreprod25.5.1009.

[39] Betteridge KJ, Fléchon JE. The anatomy and physiology of pre-attachment bovine embryos. Theriogenology 1988;29:155–87. https://doi.org/10.1016/0093-691X(88)90038-6.

[40] Houghton FD. Energy metabolism of the inner cell mass and trophectoderm of the mouse blastocyst. Differentiation 2006;74:11–8.

[41] Mishra P, Chan DC. Metabolic regulation of mitochondrial dynamics. J Cell Biol 2016;212:379–87. https://doi.org/10.1083/jcb.201511036.

[42] Gomes LC, Benedetto G Di, Scorrano L. During autophagy mitochondria elongate, are spared from degradation and sustain cell viability. Nat Cell Biol 2011;13:589–98. https://doi.org/10.1038/ncb2220.

[43] Watson AJ. Regulation of blastocyst formation. Front Biosci 2001;6:d708. https://doi.org/10.2741/watson.

[44] Wiley LM. Cavitation in the mouse preimplantation embryo: Na K-ATPase and the origin of nascent blastocoele fluid. Dev Biol 1984;105:330–42. https://doi.org/10.1016/0012-1606(84)90290-2.

[45] Marikawa Y, Alarcon VB. Creation of trophectoderm, the first epithelium, in mouse

preimplantation development. Results Probl Cell Differ 2012;55:165–84. https://doi.org/10.1007/978-3-642-30406-4-9.

[46] Rodríguez A, Diez C, Ikeda S, Royo LJ, Caamaño JN, Alonso-Montes C, et al. Retinoids during the in vitro transition from bovine morula to blastocyst. Hum Reprod 2006;21:2149–57. https://doi.org/10.1093/humrep/del099.

[47] Donnay I, Leese HJ. Embryo metabolism during the expansion of the bovine blastocyst. Mol Reprod Dev 1999;53:171–8. https://doi.org/10.1002/(SICI)1098-2795(199906)53:2<171::AID-MRD6>3.0.CO;2-F.

[48] Houghton FD, Humpherson PG, Hawkhead JA, Hall CJ, Leese HJ. Na+, K+, ATPase activity in the human and bovine preimplantation embryo. Dev Biol 2003;263:360–6. https://doi.org/10.1016/j.ydbio.2003.07.014.

[49] Zhang J, Khvorostov I, Hong JS, Oktay Y, Vergnes L, Nuebel E, et al. UCP2 regulates energy metabolism and differentiation potential of human pluripotent stem cells. EMBO J 2011;30:4860–73. https://doi.org/10.1038/emboj.2011.401.

[50] Jakobs S, Martini N, Schauss AC, Egner A, Westermann B, Hell SW. Spatial and temporal dynamics of budding yeast mitochondria lacking the division component Fis1p. J Cell Sci 2003;116:2005–14. https://doi.org/10.1242/jcs.00423.

[51] Egner A, Jakobs S, Hell SW. Fast 100-nm resolution three-dimensional microscope reveals structural plasticity of mitochondria in live yeast. Proc Natl Acad Sci U S A 2002;99:3370–5. https://doi.org/10.1073/pnas.052545099.

[52] Yao CH, Wang R, Wang Y, Kung CP, Weber JD, Patti GJ. Mitochondrial fusion supports increased oxidative phosphorylation during cell proliferation. Elife 2019;8:1–19. https://doi.org/10.7554/eLife.41351.

[53] Gopichandran N, Leese HJ. Metabolic characterization of the bovine blastocyst, inner cell mass,

trophectoderm and blastocoel fluid. Reproduction 2003;126:299–308. https://doi.org/10.1530/rep.0.1260299.

[54] Hosseini SM, Dufort I, Caballero J, Moulavi F, Ghanaei HR, Sirard MA. Transcriptome profiling of bovine inner cell mass and trophectoderm derived from in vivo generated blastocysts. BMC Dev Biol 2015;15:1–13. https://doi.org/10.1186/s12861-015-0096-3.

393 **Figure captions**

394 **Fig 1.** Measurements of major and minor axes to determine mitochondrial oblateness.
395 Regular mitochondria (A), bent mitochondria (B), mitochondria with nodes (C), and hooded
396 mitochondria (D) are represented with measurement lines (blue: major axis; red: minor axis).
397 Oblateness for each mitochondrion was calculated according to the formula described in the
398 Materials and Methods section. Bars = 500 nm.

399

400 **Fig 2.** Representative immature and mature mitochondria in the 2-cell stage embryo and cumulus
401 cell. (A) Overview of a 2-cell stage embryo. Bar = 20 μm. (B) Immature mitochondria in boxed area
402 indicated in (A). All the mitochondria are globular, with an internal vesicle. Clear cristae were not
403 observed in the mitochondria. Bar= 500 nm. (C) Overview of a cumulus cell. Bar = 2 μm. (D)
404 Mature mitochondria in the boxed area indicated in (C). All the mitochondria are elliptical or
405 elongated. Bar= 500 nm. Arrowheads indicate individual mitochondrion.

406

407 **Fig 3.** Mitochondria of a bovine blastocyst. (A) Overview of a bovine blastocyst. Bar = 20 μm. (B)
408 The boundary between the inner cell mass (ICM) and trophectoderm (TE) of the
409 blastocyst is represented by a dashed line. Bar = 500 nm. (C) Another section of mitochondria in the
410 ICM. Bar= 500 nm. (D) Another section for mitochondria in the TE. Bar= 500 nm. “M” indicates an
411 individual mitochondrion, and “HM” indicates a hooded mitochondrion in the section observed.

412

413 **Fig 4.** Morphology of mitochondrial cristae in the ICM and TE of blastocysts. Mitochondria in the
414 ICM (A) and TE (B). (C) Frequencies of cristae types in the ICM (1,781) and TE (1,405). Black
415 arrowheads indicate mitochondria with lamellar cristae. White arrowheads indicate mitochondria
416 with bleb cristae. Yellow arrowheads indicate mitochondria with immature cristae. Bar = 500 nm.

Fig 5. Evaluation of mitochondrial elongation based on the oblateness value in 2-cell stage embryos, ICM, TE, and cumulus cells.

Each dot represents the oblateness value of a single mitochondrion. Oblateness values were calculated according to the formula described in the Materials and Methods section. The black lines indicate the average values; 2-cell stage embryos (purple): 0.253, ICM (blue): 0.314; TE (red): 0.465, cumulus cells (green): 0.492. Different letters indicate a statistically significant difference ($P < 0.01$).

Supplemental Fig 1. Representative TEM image of each bovine blastocyst used for analysis.

(A) The TE and ICM regions were defined based on a boundary between TE and ICM cells as shown in this representative image. Bar = 20 μm. (B) Magnified view of the green box in (A). A boundary between ICM and TE cells is clearly identifiable. Bar = 2 μm.

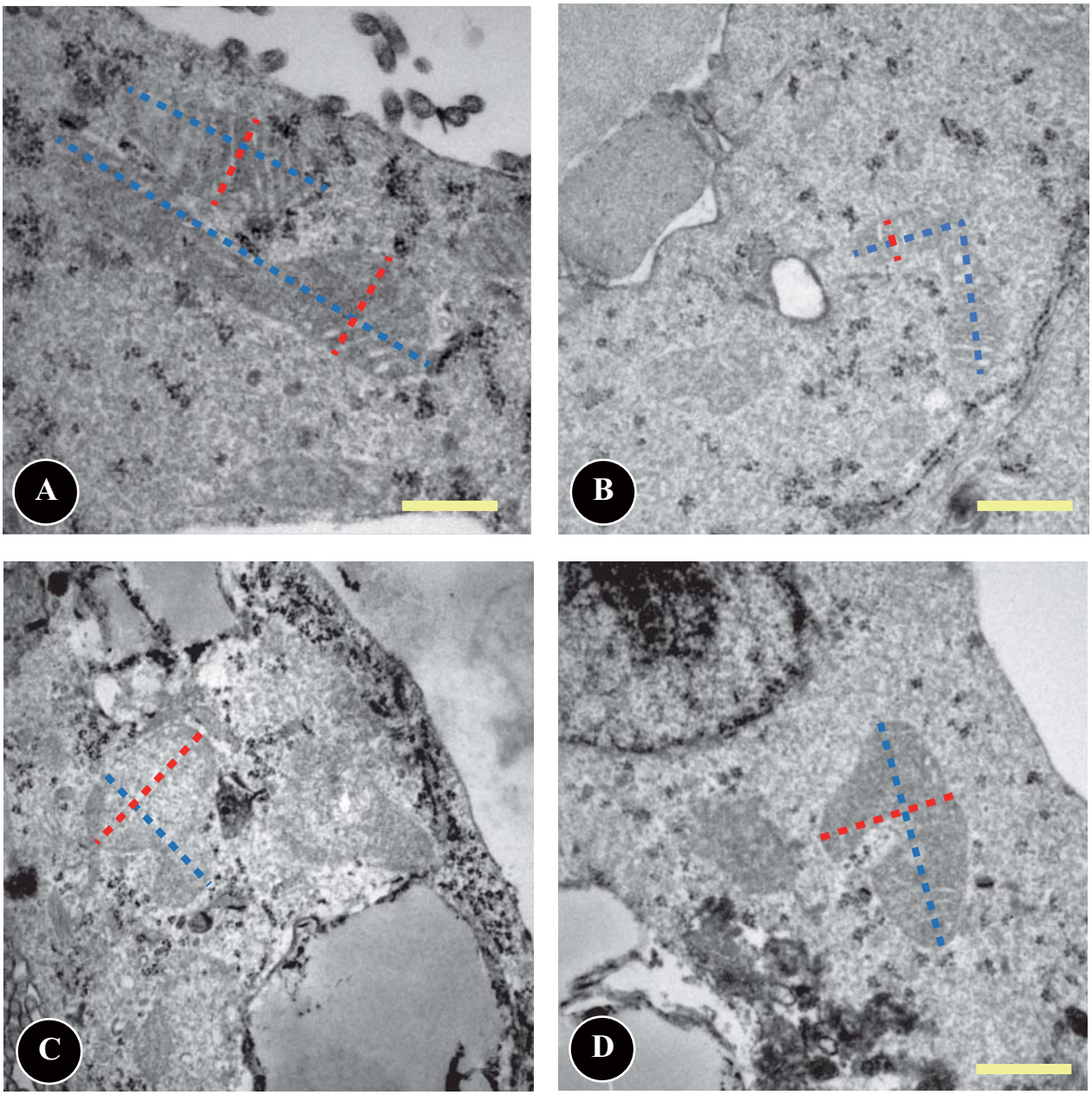

Figure 1. Measurements of major and minor axes to determine the mitochondrial oblateness. Regular mitochondria (A), bent mitochondria (B), mitochondria with nodes (C), and hooded mitochondria (D) are represented with measurement lines (blue: major axis; red: minor axis). Oblateness for each mitochondrion was calculated according to the formula described in the Materials and Methods section. Bar= 500 nm.

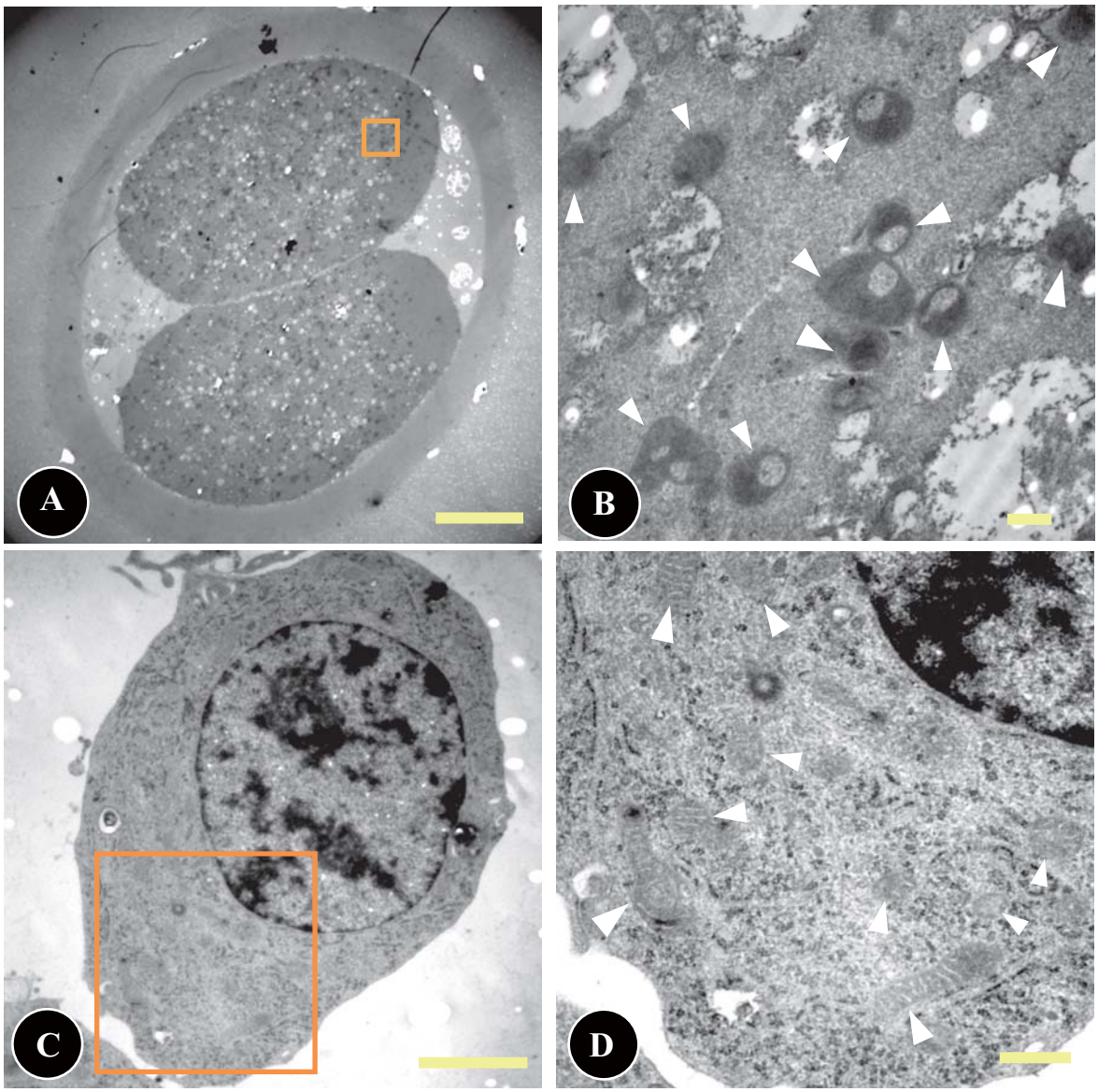

Figure 2. Representative immature and mature mitochondria in the 2-cell stage embryo and cumulus cell. (A) Overview of 2-cell stage embryo. Bar= 20 μm. (B) Immature mitochondria in the black box of (A). All the mitochondria are globular with internal vesicle. Clear cristae were not observed in those. Bar= 500 nm. (C) Overview of cumulus cell. Bar= 2 μm. (D) Mature mitochondria in the black box of (C). All the mitochondria are elliptic or elongated. Bar= 500 nm. Arrowheads indicates individual mitochondrion in the section observed.

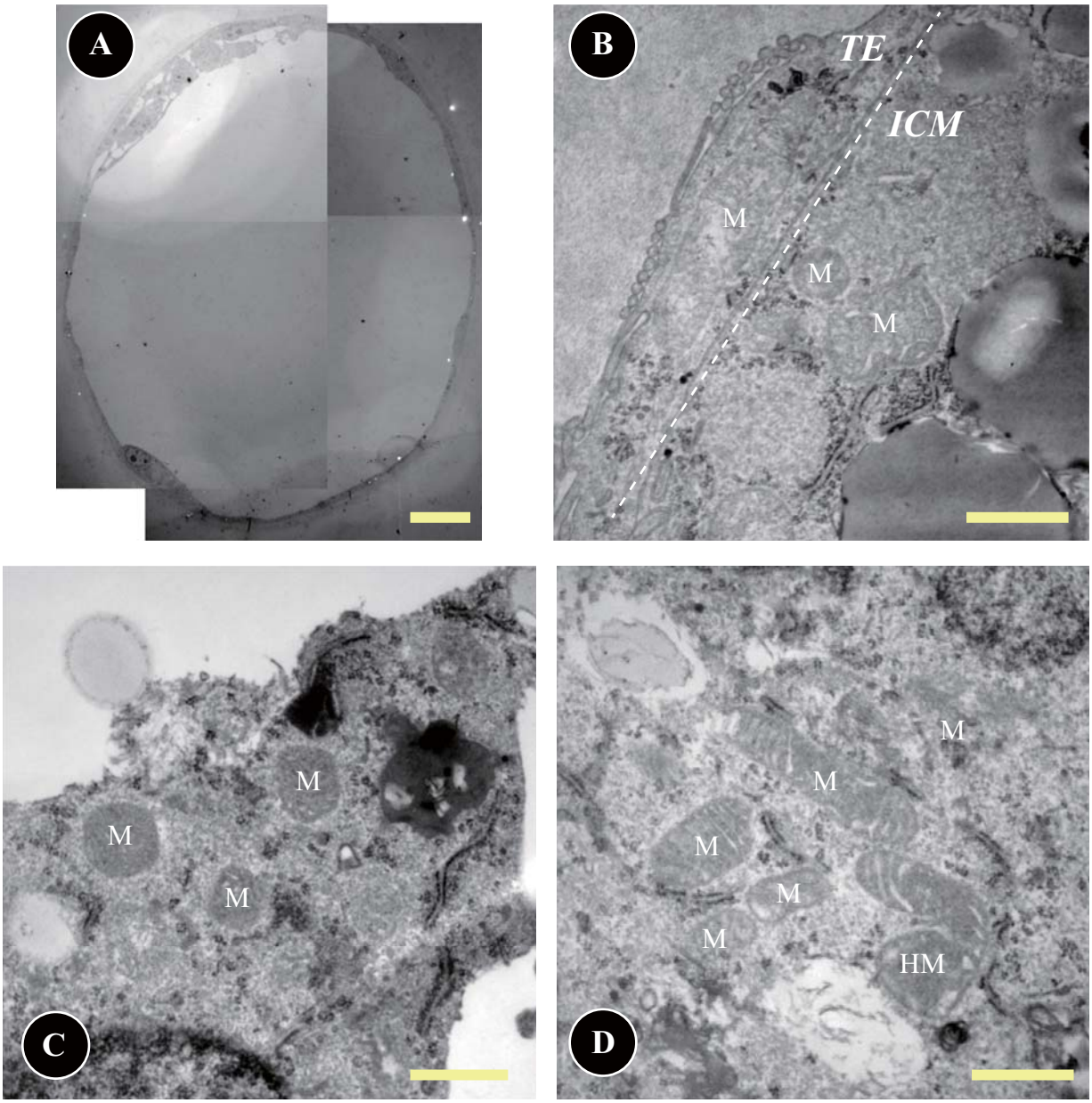

Fig 3. Mitochondria of a bovine blastocyst. (A) Overview of a bovine blastocyst. Bar = 20 μm. (B) The boundary between the inner cell mass (ICM) and trophectoderm (TE) of the blastocyst is represented by a dashed line. Bar= 500 nm. (C) Another section of mitochondria in the ICM. Bar= 500 nm. (D) Another section for mitochondria in the TE. Bar= 500 nm. "M" indicates an individual mitochondrion, and "HM" indicates a hooded mitochondrion in the section observed.

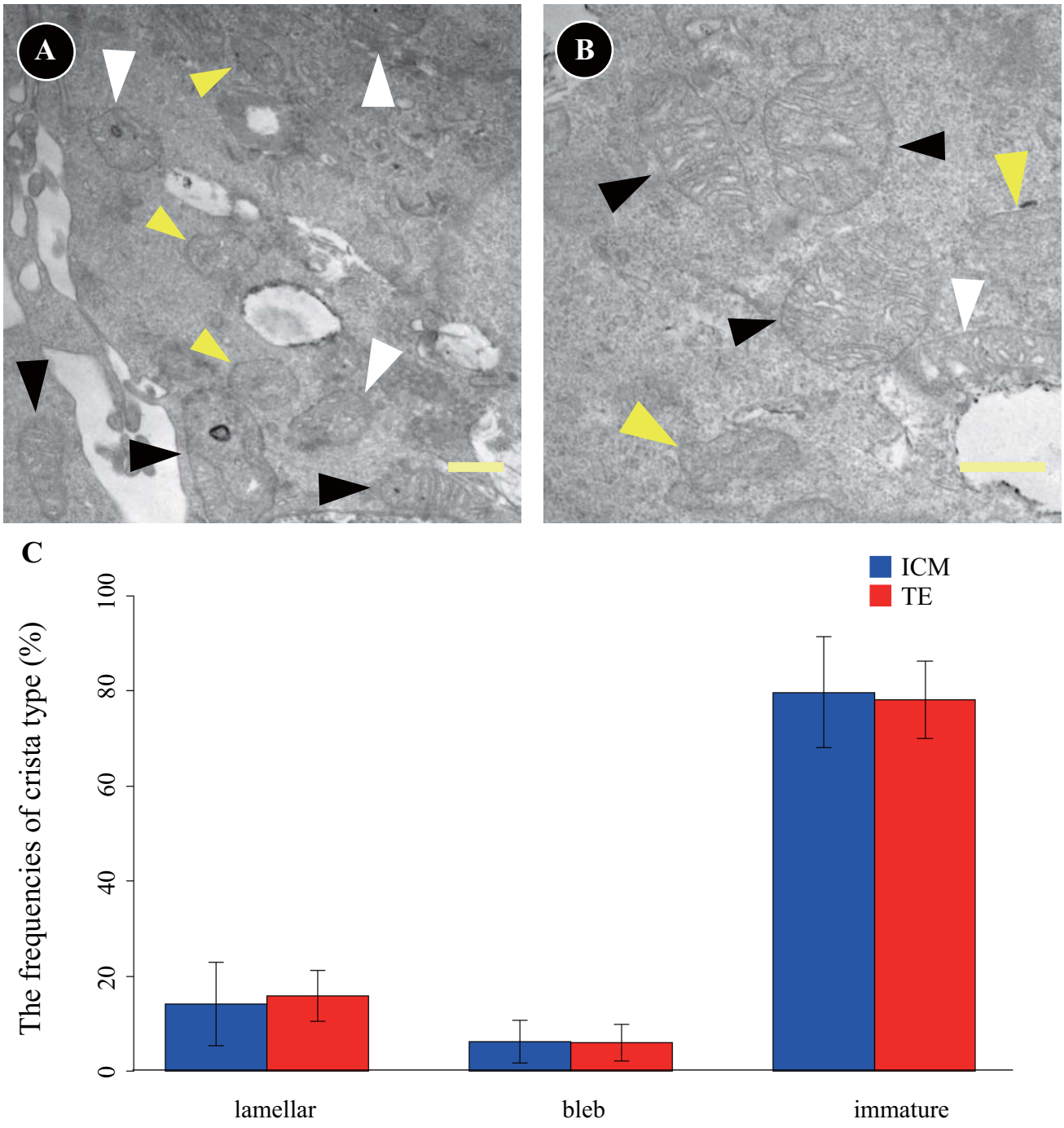

Fig. 4. Morphology of mitochondrial cristae in the ICM and TE of blastocysts. Mitochondria in the ICM (A) and TE (B). (C) Frequencies of cristae types in the ICM (1,781) and TE (1,405). Black arrowheads indicate mitochondria with lamellar cristae. White arrowheads indicate mitochondria with bleb cristae. Yellow arrowheads indicate mitochondria with immature cristae. Bar = 500 nm.

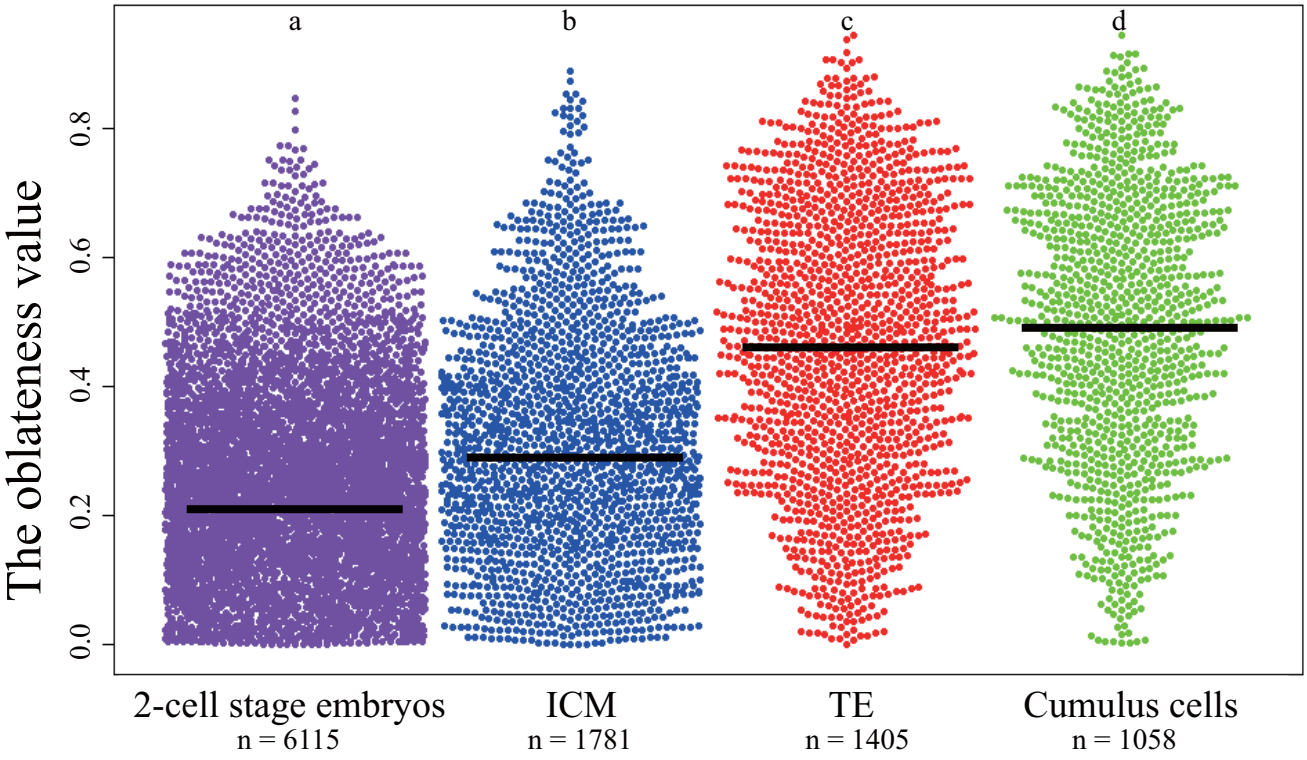

Fig 5. Evaluation of mitochondrial elongation based on the oblateness value in 2-cell stage embryos, ICM, TE, and cumulus cells. Each dot represents the oblateness value of a single mitochondrion. Oblateness values were calculated according to the formula described in the Materials and Methods section. The black lines indicate the average values; 2-cell stage embryos (purple): 0.253, ICM (blue): 0.314; TE (red): 0.465, cumulus cells (green): 0.492. Different letters indicate a statistically significant difference ($P < 0.01$).

Table. 1 The number of hooded mitochondria in the ICM and the TE of blastocysts

	ICM	TE
Total no. of mitochondria observed	1781	1405
No. of hooded mitochondria (% ± s.e.m.)	36 (2.0 ± 1.1%)	40 (2.8 ± 0.9%)

s.e.m.: standard error of the mean.

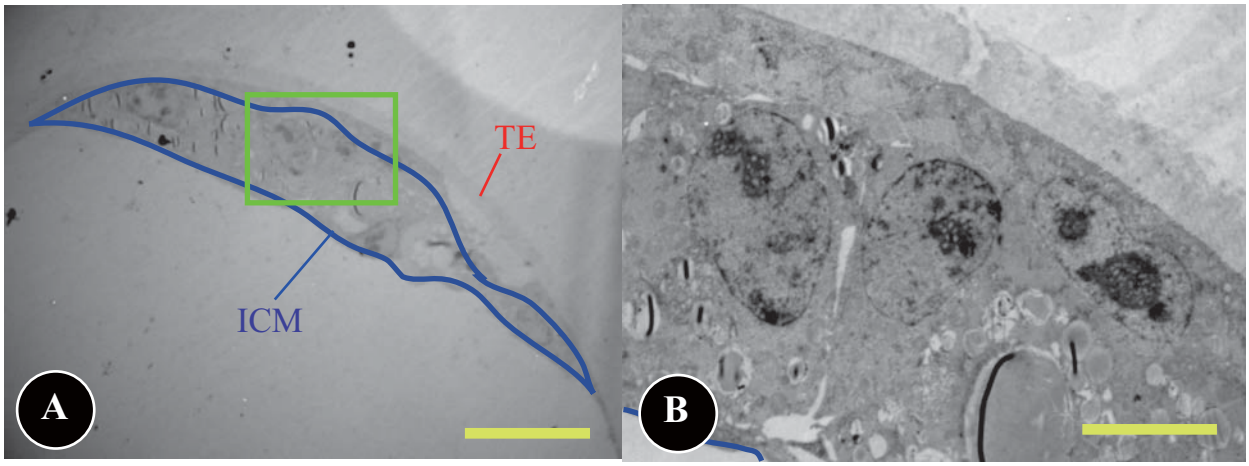

Supplemental Fig 1. Representative TEM image of bovine blastocyst used for analysis. (A) The TE and ICM regions were defined based on a border between TE and ICM cells as shown in this representative image. Bar = 20 μm. (B) Magnified view of the green box in (A). A boundary between ICM and TE cells is clearly identifiable. Bar = 2 μm.

Supplemental table. 1 Developmental rates *in vitro* of bovine IVF embryos in the present study

Number of retrieved COCs	No. of cultured embryos	No. of cleaved embryos (%)	No. of expanded blastocysts (%)
201	152	109 (71.7)	50 (32.9)